

A Gauss–Seidel Projection Method for Micromagnetics Simulations

Xiao-Ping Wang,* Carlos J. García-Cervera,† and Weinan E‡

**Department of Mathematics, The Hong Kong University of Science and Technology, Clear Water Bay, Kowloon, Hong Kong;* †*Department of Mathematics, Princeton University, Princeton, New Jersey 08544;* ‡*Courant Institute, New York University, New York, New York 10012, and Department of Mathematics and Program in Applied and Computational Mathematics, Princeton University, Princeton, New Jersey 08544*

E-mail: mawang@ust.hk, URL:<http://www.math.ust.hk/~mawang>; cgarcia@princeton.edu,

URL:<http://www.math.princeton.edu/~cgarcia>; weinan@princeton.edu,

URL:<http://www.math.princeton.edu/~weinan>

Received November 30, 2000; revised March 22, 2001

One of the main difficulties in micromagnetics simulation is the severe time step constraint introduced by the exchange field. Using standard explicit integrators leads to a physical time step of sub-pico seconds, which is often two orders of magnitude smaller than the fastest physical time scales. Direct implicit integrators require solving complicated, coupled systems. In this paper, we introduce an implicit method whose complexity is comparable to solving the scalar heat equation implicitly. This method is based on a combination of a Gauss–Seidel implementation of a fractional step implicit solver for the gyromagnetic term, and the projection method for the heat flow of harmonic maps. This method allows us to carry out fully resolved calculations for the switching of the magnetization in micron-sized elements. © 2001 Academic Press

Key Words: Landau–Lifshitz equation; micromagnetics; projection method; implicit methods.

1. INTRODUCTION

The dynamics of the magnetization distribution in a ferromagnetic thin film is an interesting and important problem from both a scientific and a technological point of view. Customarily, the main interest in these films has been their application in the magnetic recording industry. More recently, interest on using them as magnetic memory devices (MRAM) has given a greater incentive to study this subject. Since defects, impurities, and thermal noise play important roles on the dynamics of the magnetization field in films of nanometer thickness, it also makes an ideal playground for studying some of the nano-scale physics [4, 7, 8, 10, 18].

The relaxation process of the magnetization distribution in a ferromagnetic material is described by the Landau–Lifshitz equation [12, 14],

$$\mathbf{M}_t = -\gamma \mathbf{M} \times \mathcal{H} - \frac{\gamma \alpha}{M_s} \mathbf{M} \times (\mathbf{M} \times \mathcal{H}), \quad (1)$$

where $|\mathbf{M}| = M_s$ is the saturation magnetization, and is usually set to be a constant far from the Curie temperature. The first term on the right-hand side is the gyromagnetic term, with γ being the gyromagnetic ratio. The second term in the right-hand side is the damping term, with α being the dimensionless damping coefficient. The term \mathcal{H} is the local field, computed from the Landau–Lifshitz free energy functional:

$$\mathcal{H} = -\frac{\delta F}{\delta \mathbf{M}} \quad (2)$$

$$F[\mathbf{M}] = \frac{1}{2} \int_{\Omega} \left\{ \Phi\left(\frac{\mathbf{M}}{M_s}\right) + \frac{A}{M_s^2} |\nabla \mathbf{M}|^2 - 2\mu_0 \mathbf{H}_e \cdot \mathbf{M} \right\} dx + \frac{\mu_0}{2} \int_{\mathbb{R}^3} |\nabla U|^2 dx. \quad (3)$$

In (3), A is the exchange constant, $\frac{A}{M_s^2} |\nabla \mathbf{M}|^2$ is the exchange interaction energy between the spins, $\Phi\left(\frac{\mathbf{M}}{M_s}\right)$ is the energy resulting from material anisotropy, μ_0 is the permeability of vacuum ($\mu_0 = 4\pi \times 10^{-7} \text{ N/A}^2$ in the S.I.), $-2\mu_0 \mathbf{H}_e \cdot \mathbf{M}$ is the energy resulting from the external applied field, Ω is the volume occupied by the material, and finally the last term in (3) is the energy resulting from the field induced by the magnetization distribution inside the material. This induced field $\mathbf{H}_s = -\nabla U$ can be computed by solving

$$\Delta U = \begin{cases} \nabla \cdot \mathbf{M} & \text{in } \Omega \\ 0 & \text{outside } \Omega, \end{cases} \quad (4)$$

together with the jump conditions

$$\begin{aligned} [U]_{\partial\Omega} &= 0 \\ \left[\frac{\partial U}{\partial \nu} \right]_{\partial\Omega} &= -\mathbf{M} \cdot \nu \end{aligned} \quad (5)$$

at the boundary of the domain Ω . In (5) we denote by $[v]_{\partial\Omega}$ the jump of v at boundary of Ω :

$$[v]_{\partial\Omega}(x) = \lim_{\substack{y \rightarrow x \\ y \in \Omega^c}} v(y) - \lim_{\substack{y \rightarrow x \\ y \in \Omega}} v(y).$$

The solution to Eq. (4), with boundary conditions (5) is

$$\nabla U(x) = \nabla \int_{\Omega} \nabla N(x-y) \cdot \mathbf{M}(y) dy, \quad (6)$$

where $N(x) = -\frac{1}{4\pi} \frac{1}{|x|}$ is the Newtonian potential.

The gyromagnetic term in the Landau–Lifshitz equation (1) is a conservative term, whereas the damping term is dissipative.

Understanding the long-term dynamics of the Landau–Lifshitz system (1) is of practical interest in the design of effective mechanisms for switching the magnetization in computer

memory cells [4, 18]. Numerical simulation has become an important tool in the study of both static and dynamic issues in ferromagnetic materials [1, 2, 6, 9, 11, 15, 16, 19, 26]. In the simulation of the magnetization reversal process, it is important to be able to resolve the different small length scales involved, in particular, magnetic domain walls, and magnetic vortices, since these are responsible for the switching anomalies observed in experiments with submicron patterned NiFe arrays [17, 21, 22, 23, 24]. Explicit numerical schemes, such as fourth-order Runge–Kutta, or predictor–corrector schemes, with some kind of adaptive time stepping procedure, are currently the most commonly used methods for the simulation of the Landau–Lifshitz equation. Although explicit schemes may achieve high order of accuracy both in space and time, the time step size is severely constrained by the stability of the numerical scheme. For physical constants characteristic of the permalloy ($M_s = 8.0 \times 10^5$ Ampere/m, $K_u = 5.0 \times 10^2$ J/m³, $A = 1.3 \times 10^{-11}$ J/m, $\gamma = 1.76 \times 10^{11}$ T⁻¹ s⁻¹), with a cell size $\Delta x = 0.004$ μ m (256 grid points in a 1- μ m long sample), and using fourth-order Runge–Kutta, we need to use a time step roughly of the order $\Delta t \approx .25$ picoseconds for numerical stability. If the cell size is decreased by a factor of 10, the time step Δt must be reduced by a factor of 100. In addition, in a typical hysteresis loop, the change in the average magnetization with respect to the change in the applied field behaves very differently near and far from the switching field, with little change far from it, and an abrupt change as the applied field approaches the switching field. These considerations show the need of schemes for the numerical integration of the Landau–Lifshitz equation that are adaptive in time. Our first step for the construction of such a method is the construction of a numerical scheme that is unconditionally stable.

In order to overcome the stability constraint of explicit schemes, one usually resorts to implicit schemes [15]. However, because of the strong nonlinearities present in both the gyromagnetic and damping terms in the Landau–Lifshitz equation (1), a direct implicit discretization of the system is not efficient and is difficult to implement. To understand the crux of the matter, let us restrict our attention to the case when only the exchange term is kept in (2). In this case $\mathcal{H} = \Delta \mathbf{m}$ and the Landau–Lifshitz equation (1) reduces to

$$\mathbf{m}_t = -\mathbf{m} \times \Delta \mathbf{m} - \mathbf{m} \times (\mathbf{m} \times \Delta \mathbf{m}). \quad (7)$$

Our goal is to develop a stable numerical scheme for (7) which allows us to use large time steps. The gyromagnetic term and the damping term will require different treatment.

When only the damping term is present, Eq. (7) becomes

$$\mathbf{m}_t = -\mathbf{m} \times (\mathbf{m} \times \Delta \mathbf{m}) = \Delta \mathbf{m} + |\nabla \mathbf{m}|^2 \mathbf{m}. \quad (8)$$

This equation describes the heat flow for harmonic maps. In [5], a simple projection scheme was introduced for this equation. This scheme was shown to be unconditionally stable and more efficient than other schemes used for the simulation of Eq. (8).

In this paper, we will be mainly concerned with the gyromagnetic term in the Landau–Lifshitz equation:

$$\mathbf{m}_t = -\mathbf{m} \times \Delta \mathbf{m} \quad (9)$$

This equation is the symplectic flow of harmonic maps [3, 25]. We introduce a simple and efficient scheme for (9) which is also unconditionally stable. The key to this new scheme

is the observation that, because of the vectorial product structure of the equation, a Gauss–Seidel type of technique significantly improves the stability property of explicit schemes for the Landau–Lifshitz equation. This Gauss–Seidel technique is then used together with a splitting procedure to obtain an efficient and, more importantly, unconditionally stable scheme. In addition to the simplicity and unconditional stability, the scheme is also symplectic in a certain sense. Combined with the projection scheme for the damping part, we have an unconditionally stable scheme for the full Landau–Lifshitz equation.

We apply our method to the simulation of anomalous switching in patterned submicron arrays. It was observed experimentally by Jing Shi *et al.* [17, 21–24] that trapped magnetization vortices are responsible for the switching anomaly. The numerical simulation of this problem is extremely demanding. To calculate the hysteresis loop and the remanent magnetization curve, one needs to run more than 100 evolutions to steady state and, at the same time, more than 256 grid points are needed in each direction in order to resolve the vortices and domain walls.

This paper is organized as follows: In Section 2 we study the effect of the vectorial nature of the Landau–Lifshitz equation on the stability of several frequently used time stepping procedures by analyzing a simple example in detail. We introduce our Gauss–Seidel technique and make the important observation that this technique improves the stability properties of the explicit schemes. In Section 3, we introduce a fractional step procedure for (9) that takes advantage of the Gauss–Seidel technique. The analysis from the previous section suggests that our scheme is unconditionally stable. In Section 4, we compare the performance of our scheme with that of two different explicit schemes for the symplectic flow of harmonic maps. In Section 5, we combine our new method with the projection method for the heat flow of the harmonic map derived in [5], and introduce the *Gauss–Seidel Projection Method* for the full Landau–Lifshitz equation. In Section 6 we review some of the switching anomaly experiments, and present numerical simulations performed using the Gauss–Seidel Projection Method. We are able to resolve the vortex dynamics and accurately simulate the switching anomaly observed in [17, 21–24].

2. A SIMPLE EXAMPLE: $\frac{d\mathbf{m}}{dt} = -\mathbf{a} \times \mathbf{m}$

The vectorial structure of the Landau–Lifshitz equation (1) presents some interesting features when time stepping schemes are considered. To appreciate this, let us first consider the simple linear vectorial equation

$$\frac{d\mathbf{m}}{dt} = -\mathbf{a} \times \mathbf{m}, \quad (10)$$

where $\mathbf{a}^T = (a_1, a_2, a_3)$ is a constant vector.

2.1. Standard One-Step Methods

The forward Euler scheme for equation (10) is

$$\mathbf{m}^{n+1} = \mathbf{m}^n - \Delta t(\mathbf{a} \times \mathbf{m}^n), \quad (11)$$

or, in its component form,

$$\begin{pmatrix} m_1^{n+1} \\ m_2^{n+1} \\ m_3^{n+1} \end{pmatrix} = \begin{pmatrix} m_1^n - \Delta t (a_2 m_3^n - a_3 m_2^n) \\ m_2^n - \Delta t (a_3 m_1^n - a_1 m_3^n) \\ m_3^n - \Delta t (a_1 m_2^n - a_2 m_1^n) \end{pmatrix} = A \begin{pmatrix} m_1^n \\ m_2^n \\ m_3^n \end{pmatrix}, \quad (12)$$

where Δt is the time step size, and

$$A = \begin{pmatrix} 1 & \tilde{a}_3 & -\tilde{a}_2 \\ -\tilde{a}_3 & 1 & \tilde{a}_1 \\ \tilde{a}_2 & -\tilde{a}_1 & 1 \end{pmatrix}, \quad \tilde{a}_i = a_i \Delta t.$$

To discuss the stability of the Euler scheme, we compute the characteristic polynomial of A

$$\det(A - \lambda I) = (1 - \lambda)^3 + (1 - \lambda)(a_1^2 + a_2^2 + a_3^2)(\Delta t)^2.$$

The three eigenvalues are $\lambda_0 = 1$, $\lambda_{\pm} = 1 \pm |a|\Delta t i$. Thus, the spectral radius $\rho(A) = \sqrt{1 + |a|^2(\Delta t)^2} > 1$, which implies that the stability region for the Euler scheme contains only one point (i.e., $\Delta t = 0$).

Similar calculations show the same feature for the second-order Runge–Kutta scheme. However, for the fourth-order Runge–Kutta scheme, the three eigenvalues for the characteristic polynomial satisfy $|\lambda_0| = 1$, $|\lambda_{\pm}| = 1 - \frac{1}{72}(|a|\Delta t)^6 + \frac{1}{(24)^2}(|a|\Delta t)^8$, and we have that $\rho(A) \leq 1$ provided that $\Delta t \leq \frac{\sqrt{8}}{|a|}$.

This phenomenon is easy to understand. The spectrum of the system of ordinary differential equations (10), $\lambda = \{-|a|i, 0, |a|i\}$, lies on the imaginary axis. It is well known that the stability regions of the forward Euler and second-order Runge–Kutta schemes do not contain any part of the imaginary axis except the origin. On the other hand, the stability regions of the classical third- and fourth-order Runge–Kutta schemes do contain part of the imaginary axis. This leads to the condition of absolute stability $\Delta t \leq \frac{\sqrt{8}}{|a|}$ for the fourth-order Runge–Kutta scheme.

2.2. The Gauss–Seidel Approach

We have shown that the usual forward Euler scheme is unstable for the linear equation

$$\frac{d\mathbf{m}}{dt} = -\mathbf{a} \times \mathbf{m}.$$

Let us consider the following Gauss–Seidel correction to (11) and (12):

$$\begin{pmatrix} m_1^{n+1} \\ m_2^{n+1} \\ m_3^{n+1} \end{pmatrix} = \begin{pmatrix} m_1^n - \Delta t (a_2 m_3^n - a_3 m_2^n) \\ m_2^n - \Delta t (a_3 m_1^{n+1} - a_1 m_3^n) \\ m_3^n - \Delta t (a_1 m_2^{n+1} - a_2 m_1^{n+1}) \end{pmatrix}. \quad (13)$$

We can rewrite (13) as

$$\begin{pmatrix} 1 & 0 & 0 \\ \tilde{a}_3 & 1 & 0 \\ -\tilde{a}_2 & \tilde{a}_1 & 1 \end{pmatrix} \begin{pmatrix} m_1^{n+1} \\ m_2^{n+1} \\ m_3^{n+1} \end{pmatrix} = \begin{pmatrix} 1 & \tilde{a}_3 & -\tilde{a}_2 \\ 0 & 1 & \tilde{a}_1 \\ 0 & 0 & 1 \end{pmatrix} \begin{pmatrix} m_1^n \\ m_2^n \\ m_3^n \end{pmatrix} \quad (14)$$

or

$$\begin{aligned} \begin{pmatrix} m_1^{n+1} \\ m_2^{n+1} \\ m_3^{n+1} \end{pmatrix} &= \begin{pmatrix} 1 & \tilde{a}_3 & -\tilde{a}_2 \\ -\tilde{a}_3 & 1 - \tilde{a}_3^2 & \tilde{a}_1 + \tilde{a}_2\tilde{a}_3 \\ \tilde{a}_1\tilde{a}_3 + \tilde{a}_2 & \tilde{a}_1\tilde{a}_3^2 + \tilde{a}_2\tilde{a}_3 - \tilde{a}_1 & 1 - \tilde{a}_1\tilde{a}_2\tilde{a}_3 - \tilde{a}_1^2 - \tilde{a}_2^2 \end{pmatrix} \begin{pmatrix} m_1^n \\ m_2^n \\ m_3^n \end{pmatrix} \\ &= A \begin{pmatrix} m_1^n \\ m_2^n \\ m_3^n \end{pmatrix} \end{aligned} \quad (15)$$

The eigenvalues of the transition matrix A are

$$\lambda_0 = 1, \quad \lambda_{\pm} = 1 - b \pm \sqrt{b(b-2)},$$

where $b = \frac{1}{2}(|a|^2 + a_1a_2a_3\Delta t)(\Delta t)^2$. It is easy to see that when $0 < b < 2$, or roughly

$$\Delta t < \frac{2}{|a|},$$

the three eigenvalues are different and $|\lambda_{\pm}| = 1$.

The transition matrix A has the following property, for $0 < b < 2$: There exists an invertible matrix T such that

$$A = T^{-1} \begin{pmatrix} 1 & 0 & 0 \\ 0 & 1-b & \sqrt{b(2-b)} \\ 0 & -\sqrt{b(2-b)} & 1-b \end{pmatrix} T = T^{-1} \begin{pmatrix} 1 & 0 \\ 0 & S \end{pmatrix} T.$$

Here

$$S = \begin{pmatrix} 1-b & \sqrt{b(2-b)} \\ -\sqrt{b(2-b)} & 1-b \end{pmatrix}$$

is a symplectic matrix in the sense that $S^T J S = J$, where

$$J = \begin{pmatrix} 0 & 1 \\ -1 & 0 \end{pmatrix}.$$

Thus, (13) is a natural extension to odd-dimensions of the symplectic schemes proposed in [13]. See also [20].

3. AN IMPLICIT GAUSS-SEIDEL SCHEME FOR THE LANDAU-LIFSHITZ EQUATION WITHOUT DAMPING

3.1. A Fractional Step Procedure

We consider the equation

$$\mathbf{m}_t = -\mathbf{m} \times \Delta \mathbf{m}. \tag{16}$$

To overcome the nonlinearity of the equation, we consider a simple fractional step scheme

$$\begin{aligned} \frac{\mathbf{m}^* - \mathbf{m}^n}{\Delta t} &= \Delta_h \mathbf{m}^* \\ \mathbf{m}^{n+1} &= \mathbf{m}^n - \mathbf{m}^n \times \mathbf{m}^* \end{aligned} \tag{17}$$

or

$$\mathbf{m}^{n+1} = \mathbf{m}^n - \mathbf{m}^n \times (I - \Delta t \Delta_h)^{-1} \mathbf{m}^n. \tag{18}$$

Here I is the identity matrix, and Δ_h represents an approximation to the laplacian. In our code we used the standard five point approximation.

The advantage of the scheme (18) is that the implicit step is now linear, comparable to solving heat equations implicitly, and is easy to implement. It is easy to check that the scheme (18) is consistent with (16) and is first-order accurate in time. However, direct numerical implementation of (18) shows that the scheme is unstable. It is not hard to understand where the instability comes from. If one linearizes the difference scheme, (18) resembles the forward Euler scheme studied in the previous section, which is unstable when applied to a partial differential equation such as (17). Just as in the linear case, we will show that the scheme can be improved by the Gauss-Seidel technique.

3.2. The Gauss-Seidel Approach

Consider again the equation

$$\mathbf{m}_t = -\mathbf{m} \times \Delta \mathbf{m}.$$

Let

$$g_i^n = (I - \Delta t \Delta_h)^{-1} m_i^n, \quad i = 1, 2, 3. \tag{19}$$

Consider

$$\begin{pmatrix} m_1^{n+1} \\ m_2^{n+1} \\ m_3^{n+1} \end{pmatrix} = \begin{pmatrix} m_1^n + (g_2^n m_3^n - g_3^n m_2^n) \\ m_2^n + (g_3^n m_1^{n+1} - g_1^{n+1} m_3^n) \\ m_3^n + (g_1^{n+1} m_2^{n+1} - g_2^{n+1} m_1^{n+1}) \end{pmatrix} \tag{20}$$

or

$$\begin{pmatrix} 1 & 0 & 0 \\ -g_3^n & 1 & 0 \\ g_2^{n+1} & -g_1^{n+1} & 1 \end{pmatrix} \begin{pmatrix} m_1^{n+1} \\ m_2^{n+1} \\ m_3^{n+1} \end{pmatrix} = \begin{pmatrix} 1 & -g_3^n & g_2^n \\ 0 & 1 & -g_1^{n+1} \\ 0 & 0 & 1 \end{pmatrix} \begin{pmatrix} m_1^n \\ m_2^n \\ m_3^n \end{pmatrix}. \tag{21}$$

The exact stability property of the scheme (21) is difficult to analyze. Numerical experimentation suggests that the scheme is unconditionally stable.

4. COMPARISON OF THE PERFORMANCE OF VARIOUS SCHEMES

In this section we compare the performance of three different time stepping schemes for a one-dimensional Landau–Lifshitz equation with no damping:

$$\mathbf{m}_t = -\mathbf{m} \times \mathbf{m}_{xx}. \tag{22}$$

Let

$$\mathbf{m}_e = (\cos(x^2(1-x)^2)\sin(t), \sin(x^2(1-x)^2)\sin(t), \cos(t)) \tag{23}$$

be an exact solution of (22) with a forcing term $\mathbf{f} = \mathbf{m}_{et} + \mathbf{m}_e \times \mathbf{m}_{e,xx}$. The numerical solution of (22) with Neumann boundary conditions on $[0, 1]$ will be computed by the following three schemes.

1. The forward Euler scheme:

$$\begin{pmatrix} m_1^{n+1} \\ m_2^{n+1} \\ m_3^{n+1} \end{pmatrix} = \begin{pmatrix} m_1^n + \Delta t ((\Delta_h m_2^n) m_3^n - (\Delta_h m_3^n) m_2^n) \\ m_2^n + \Delta t ((\Delta_h m_3^n) m_1^n - (\Delta_h m_1^n) m_3^n) \\ m_3^n + \Delta t ((\Delta_h m_1^n) m_2^n - (\Delta_h m_2^n) m_1^n) \end{pmatrix}. \tag{FE}$$

2. An explicit Gauss–Seidel scheme:

$$\begin{pmatrix} m_1^{n+1} \\ m_2^{n+1} \\ m_3^{n+1} \end{pmatrix} = \begin{pmatrix} m_1^n + \Delta t ((\Delta_h m_2^n) m_3^n - (\Delta_h m_3^n) m_2^n) \\ m_2^n + \Delta t ((\Delta_h m_3^n) m_1^{n+1} - (\Delta_h m_1^{n+1}) m_3^n) \\ m_3^n + \Delta t ((\Delta_h m_1^{n+1}) m_2^{n+1} - (\Delta_h m_2^{n+1}) m_1^{n+1}) \end{pmatrix}. \tag{EGS}$$

This is a direct application of the Gauss–Seidel technique to the forward Euler scheme. That is, we use the recently updated information for m_1^{n+1}, m_2^{n+1} in the second and third equations.

3. The implicit Gauss–Seidel scheme

$$\begin{pmatrix} m_1^{n+1} \\ m_2^{n+1} \\ m_3^{n+1} \end{pmatrix} = \begin{pmatrix} m_1^n + (g_2^n m_3^n - g_3^n m_2^n) \\ m_2^n + (g_3^n m_1^{n+1} - g_1^{n+1} m_3^n) \\ m_3^n + (g_1^{n+1} m_2^{n+1} - g_2^{n+1} m_1^{n+1}) \end{pmatrix}, \tag{IGS}$$

$$g_i^n = (I - \Delta t \Delta_h)^{-1} m_i^n, \quad i = 1, 2, 3.$$

We first compare the stability constraints for the three schemes. For each scheme, we try to find the maximum Δt corresponding to three different spatial grid sizes Δx so that stable solutions can be computed up to $T = 0.02$. The results are shown in Table I. For the Forward Euler scheme, Δt has to be extremely small to get a stable solution up to $T = 0.02$. The explicit Gauss–Seidel scheme is much more stable but is constrained by the standard CFL condition with a CFL constant $C = 0.4$. Our implicit Gauss–Seidel scheme seems to be unconditionally stable.

TABLE I
Stability Constraint of Δt for the Three Schemes

| | FE | EGS | IGS |
|---------------------|-----------------------------------|-------------------------------------|----------------|
| $\Delta x = 0.01$ | $\Delta t \leq 1. \times 10^{-6}$ | $\Delta t \leq 4. \times 10^{-5}$ | |
| $\Delta x = 0.005$ | $\Delta t \leq 5. \times 10^{-8}$ | $\Delta t \leq 1. \times 10^{-5}$ | No restriction |
| $\Delta x = 0.0025$ | $\Delta t \leq 5. \times 10^{-9}$ | $\Delta t \leq 0.25 \times 10^{-6}$ | |

We also compare the accuracy of the three schemes. In Table II, we compare the numerical error $e(t)$ at different times for the three schemes, and for the same spatial and temporal resolutions ($\Delta x = 0.01$, $\Delta t = 10^{-6}$). Here $e(t) = \max |m_h - m_e|$ with m_e being the exact solution and m_h the numerical solution. Again, the results show that the implicit Gauss–Seidel method is the most accurate scheme among the three considered here.

5. AN IMPLICIT GAUSS–SEIDEL PROJECTION SCHEME FOR THE FULL LANDAU–LIFSHITZ EQUATION

For the full Landau–Lifshitz equation (1), we couple the above implicit Gauss–Seidel scheme with the projection method developed earlier in [5], in a fractional step framework. Since \mathbf{M} and \mathcal{H} have the same physical dimensions, we can write $\mathcal{H} = M_s \mathbf{h}$, $\mathbf{H}_s = M_s \mathbf{h}_s$, $\mathbf{H}_e = M_s \mathbf{h}_e$, and $\mathbf{M} = M_s \mathbf{m}$. Without loss of generality, we will assume that the material is uniaxial, and $\Phi(\mathbf{m}) = K_u(m_2^2 + m_3^2)$. Equation (1) is rewritten as

$$\mathbf{m}_t = -\mu_0 \gamma M_s \mathbf{m} \times \mathbf{h} - \mu_0 \gamma M_s \alpha \mathbf{m} \times \mathbf{m} \times \mathbf{h}, \quad (24)$$

where

$$\mathbf{h} = -\frac{K_u}{\mu_0 M_s^2} (m_2 \mathbf{e}_2 + m_3 \mathbf{e}_3) + \frac{A}{\mu_0 M_s^2} \Delta \mathbf{m} + \mathbf{h}_s + \mathbf{h}_e. \quad (25)$$

Here we use the notation $\mathbf{e}_1 = (1, 0, 0)$, $\mathbf{e}_2 = (0, 1, 0)$, and $\mathbf{e}_3 = (0, 0, 1)$.

The constant $\mu_0 \gamma M_s$ has dimensions of the reciprocal of time (s^{-1}). Therefore we rescale in time: $t \rightarrow (\mu_0 \gamma M_s)^{-1} t$, and we rescale the spatial variable $x \rightarrow Lx$ where L is the diameter of Ω . The equation becomes

$$\mathbf{m}_t = -\mathbf{m} \times \mathbf{h} - \alpha \mathbf{m} \times \mathbf{m} \times \mathbf{h}, \quad (26)$$

TABLE II
Accuracy of the Three Schemes ($\Delta x = 0.01$, $\Delta t = 10^{-6}$)

| | FE $\ \mathbf{m}_h - \mathbf{m}_e\ _\infty$ | EGS $\ \mathbf{m}_h - \mathbf{m}_e\ _\infty$ | IGS $\ \mathbf{m}_h - \mathbf{m}_e\ _\infty$ |
|-------------|--|---|---|
| T = 4.0D-03 | 1.5514857223D-06 | 6.4438079370D-06 | 4.7872164673D-08 |
| T = 8.0D-03 | 4.6784038819D-06 | 1.0269519915D-05 | 1.1169120310D-07 |
| T = 1.2D-02 | 8.9295719960D-06 | 1.4730269481D-05 | 1.9962607804D-07 |
| T = 1.6D-02 | 1.3785291106D-05 | 2.0275813101D-05 | 3.0626365978D-07 |
| T = 2.0D-02 | 5.1322251994D-05 | 2.3875530795D-05 | 4.0416547462D-07 |

where

$$\mathbf{h} = -Q(m_2\mathbf{e}_2 + m_3\mathbf{e}_3) + \epsilon\Delta\mathbf{m} + \mathbf{h}_s + \mathbf{h}_e. \quad (27)$$

Here we have defined the dimensionless parameters $Q = K_u/(\mu_0 M_s^2)$, and $\epsilon = A/(\mu_0 M_s^2 L^2)$.

For our splitting procedure, we define the vector field:

$$\mathbf{f} = -Q(m_2\mathbf{e}_2 + m_3\mathbf{e}_3) + \mathbf{h}_s + \mathbf{h}_e. \quad (28)$$

We solve equation

$$\mathbf{m}_t = -\mathbf{m} \times (\epsilon\Delta\mathbf{m} + \mathbf{f}) - \alpha\mathbf{m} \times \mathbf{m} \times (\epsilon\Delta\mathbf{m} + \mathbf{f}) \quad (29)$$

in three steps:

Step 1: Implicit Gauss–Seidel:

$$g_i^n = (I - \epsilon\Delta t\Delta_h)^{-1}(m_i^n + \Delta t f_i^n), \quad (30)$$

$$g_i^* = (I - \epsilon\Delta t\Delta_h)^{-1}(m_i^* + \Delta t f_i^n), \quad i = 1, 2, 3$$

$$\begin{pmatrix} m_1^* \\ m_2^* \\ m_3^* \end{pmatrix} = \begin{pmatrix} m_1^n + (g_2^n m_3^n - g_3^n m_2^n) \\ m_2^n + (g_3^n m_1^n - g_1^n m_3^n) \\ m_3^n + (g_1^n m_2^n - g_2^n m_1^n) \end{pmatrix}. \quad (31)$$

Step 2: Heat flow without constraints:

$$\mathbf{f}^* = -Q(m_2^*\mathbf{e}_2 + m_3^*\mathbf{e}_3) + \mathbf{h}_s^n + \mathbf{h}_e \quad (32)$$

$$\begin{pmatrix} m_1^{**} \\ m_2^{**} \\ m_3^{**} \end{pmatrix} = \begin{pmatrix} m_1^* + \alpha\Delta t(\epsilon\Delta_h m_1^{**} + f_1^*) \\ m_2^* + \alpha\Delta t(\epsilon\Delta_h m_2^{**} + f_2^*) \\ m_3^* + \alpha\Delta t(\epsilon\Delta_h m_3^{**} + f_3^*) \end{pmatrix}. \quad (33)$$

Step 3: Projection onto S^2 :

$$\begin{pmatrix} m_1^{n+1} \\ m_2^{n+1} \\ m_3^{n+1} \end{pmatrix} = \frac{1}{|m^{**}|} \begin{pmatrix} m_1^{**} \\ m_2^{**} \\ m_3^{**} \end{pmatrix}. \quad (34)$$

Note that the stray field is not recomputed using the intermediate values of \mathbf{m} in (30) and (32), but it is computed only once per time step.

6. APPLICATION TO THE SWITCHING ANOMALY PROBLEM

In the series of articles [17, 21–24], an experimental study of the magnetization reversal in submicron patterned arrays of 200 Å thick NiFe and NiFeCo elements was carried out. A switching anomaly was reported, and it was found to be related to the presence of trapped

magnetization vortices. The presence of trapped vortices can be detected by comparing a hysteresis loop with its corresponding remanent loop.

The hysteresis loop is obtained in the following way: Initially, a positive field of strength H_0 is applied, and the magnetization is allowed to reach a steady state. Once this steady state is reached, the applied field is reduced by a certain amount, and the sample is again allowed to reach a steady state. The process continues until we reach a negative field of strength H_0 . Then the process is repeated, increasing the field in small steps until we reach the initial applied field. The hysteresis loop is a plot of the average magnetization at the steady state as a function of the applied field strength.

For the remanent loop, an initial positive field is applied. Once a steady state is reached, the positive field is switched off, and a negative small field is applied. Once the sample reaches a steady state, the negative field is switched off, and the sample is allowed to relax to a steady state, which is a remanent state. Then the average magnetization is measured. Another (stronger) negative field is applied, and it is switched off when the sample reaches a steady state. The process continues until we reach a prescribed negative value of the applied field. For both the hysteresis and remanent loops, the increments in the applied field were constant.

A typical remanent loop can be seen in Fig. 1. The loop is characterized by two jumps and three flat pieces. The flat regions correspond to reversible changes in the magnetization: when the external field is removed, the magnetization relaxes back to the initial configuration. The jumps correspond to irreversible changes. Each flat piece in the remanent loop identifies a different stage in the reversal process. These intermediate states are responsible for the switching anomaly reported in [17, 21–24].

To simulate the reversal process, we carried out simulations of the Landau–Lifshitz equation using the Gauss–Seidel Projection Method described in the previous section. In our implementation, we divided the computational domain into cells, and in each cell we approximated the magnetization by a constant value. We also approximated the stray field

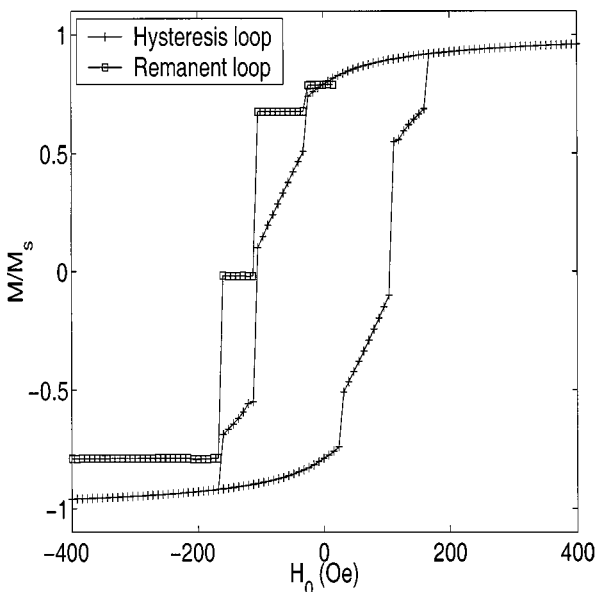


FIG. 1. Hysteresis loop and Remanent loop for the S state; the magnetization reversal occurs at about -150 Oe.

by its average value in each cell. This stray field was computed by approximating \mathbf{M} by a piecewise constant distribution, and computing the corresponding sum in (6) using Fast Fourier Transform (FFT).

The Helmholtz-type equations that appear in steps 1 and 2 were solved via an FFT-based Fast Poisson Solver: We applied the FFT in one direction, and the remaining tridiagonal system of equations was solved via Gauss elimination. The computational cost of our method is approximately one third of the computational cost of the standard fourth-order Runge–Kutta, per time step. In addition, we are able to use a time step which is an order of magnitude larger than the time step necessary for stability of the standard fourth-order Runge–Kutta.

We considered a sample of dimensions $1 \mu\text{m} \times 1 \mu\text{m} \times 200 \text{ \AA}$. We ran our code with both 256 and 512 grid points in the in-plane directions, with $\Delta t = 2$ picoseconds. The loops obtained using 256^2 and 512^2 grid points were virtually identical. The damping coefficient was fixed at $\alpha = 0.1$. The maximum field applied was $H_0 = 400 \text{ Oe}$, and the field was tilted one degree with respect to the x -axis in order to break the symmetry.

In the absence of an external field, two equilibrium states, commonly known as S state and C state, have been observed experimentally. The S state is shown in Fig. 2(a), and the C state is shown in Fig. 4(a). Figure 1 shows the hysteresis and remanent loops for an S state configuration, and Fig. 3 shows the loops for a C state.

The remanent loop in Fig. 1 clearly identifies two steps in the reversal of an S state. The flat region with near zero averaged magnetization indicates the presence of an intermediate stage in the reversal process. This stage is shown in Fig. 2(b) and is characterized by the presence of a boundary layer where the reversal has not yet occurred. The transition between the S state and this intermediate state occurs at about -100 Oe . In the second stage, the boundary layer disappears, and the reversal is complete. This occurs at about -170 Oe .

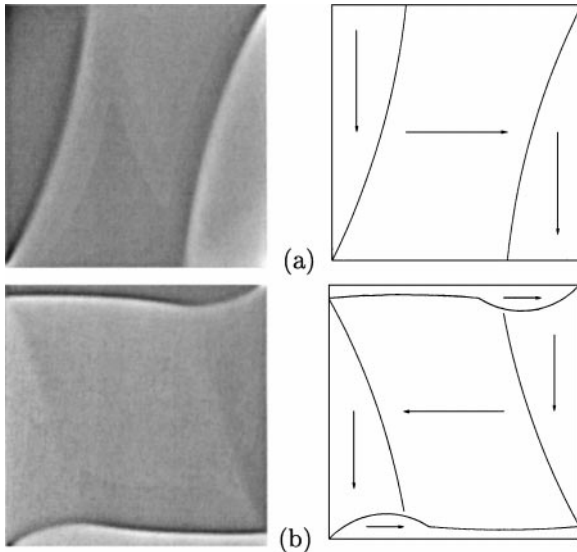


FIG. 2. Steady state configurations found in the reversal of an S state; the left column shows the divergence of the in-plane components of the magnetization. The right column is a sketch of the same configuration, showing the direction of the magnetization. (a) S state; (b) Intermediate state: the reversal has occurred in the interior, but the boundary has not switched yet.

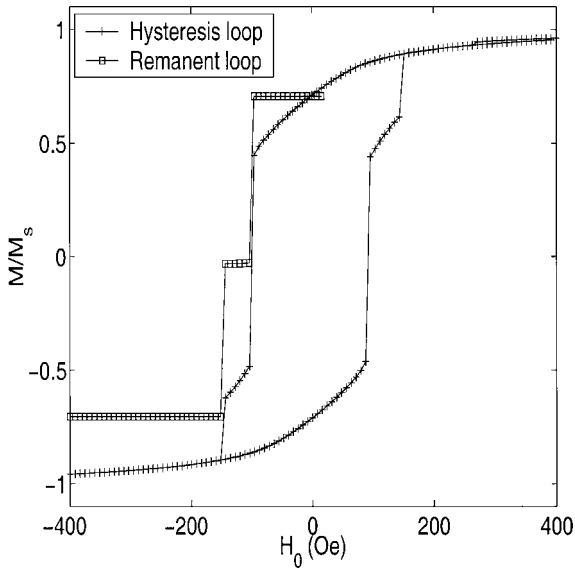


FIG. 3. Hysteresis loop and Remanent loop for the C state; the reversal occurs in three steps; at about -100 Oe, a vortex appears in the sample, and it is expelled at about -170 Oe.

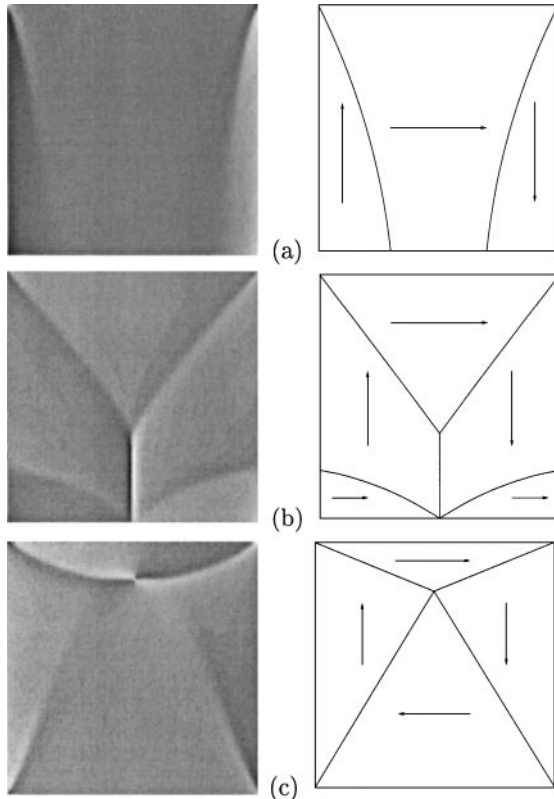


FIG. 4. Steady state configurations found in the reversal of a C state; the left column shows the divergence of the in-plane components of the magnetization. The right column is a sketch of the same configuration, showing the direction of the magnetization. (a) C state; (b) intermediate state; (c) vortex nucleated in the interior of the domain.

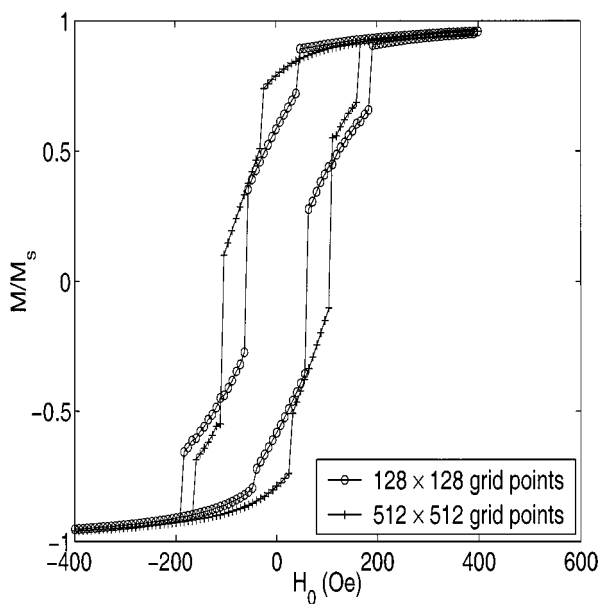


FIG. 5. Hysteresis loops for the reversal of a C state. Only 128 grid points were used in each direction, which is not enough to resolve the vortex. As a consequence, the critical fields are not captured accurately.

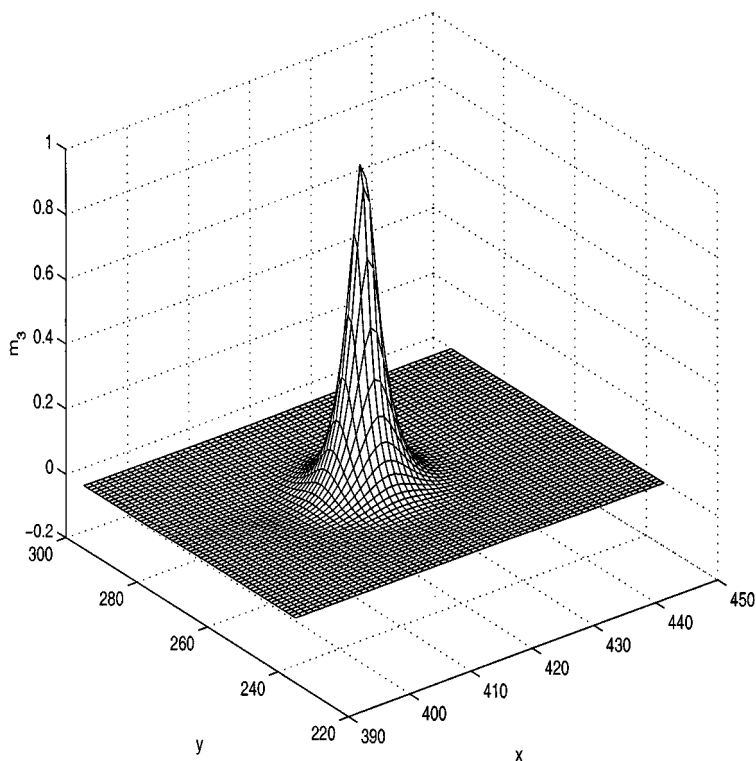


FIG. 6. A detailed view of the out-of-plane component of the magnetization in the vortex nucleated in the domain during the magnetization reversal process.

The remanent loop in Fig. 3 identifies two different stages in the reversal of a C state. The first intermediate state is shown in Fig. 4(b), and is characterized by the collapse of the left and right end domains of the C state. The transition between the C state and this state occurs at about -30 Oe. The second intermediate state is shown in Fig. 4(c), and is characterized by the nucleation of a trapped magnetization vortex. The transition occurs at about -90 Oe. An applied field of about -170 Oe is needed to expel the vortex, and complete the switching. In the numerical simulation of the reversal process, it was necessary to resolve the core of the vortices. To illustrate this, we compare in Fig. 5 a hysteresis loop computed for a C state using only 128 grid points in each direction, with the loop computed with 512 grid points in each direction. With 128 points, the core of the vortex is not well resolved. The number of steps in the magnetization reversal process is the same in both computations, and the type of steady states that we obtain is the same. Even though the vortex is nucleated in the two simulations, the dynamics of the vortex are not captured correctly when using 128 points. As a result, the transition fields are not computed accurately. In Fig. 6 we show a detailed view of the out-of-plane component of the magnetization in the vortex nucleated in the interior of the domain during the magnetization reversal process, computed with 512 grid points in each direction.

In conclusion, we have introduced a simple, efficient, and unconditionally stable scheme for the time integration of the Landau–Lifshitz equation. The complexity of our scheme is comparable to that of solving the linear heat equation with an implicit scheme. This method allows us to resolve the core of the vortices nucleated in the interior of the domain during the magnetization reversal process.

ACKNOWLEDGMENTS

We thank Roger Koch, Jing Shi, and Felix Otto for helpful discussions. The work of Weinan E was supported in part by NSF via a PECASE award. The work of X. P. Wang was supported in part by RGC Competitive Earmarked Research Grant HKUST 6176/99P.

REFERENCES

1. H. N. Bertram and C. Seberino, Numerical simulations of hysteresis in longitudinal magnetic tape, *J. Magn. Magn. Mater.* **193**, 388 (1999).
2. J. L. Blue and M. R. Scheinfein, Using multipoles decreases computation time for magnetic self-energy, *IEEE Trans. Magn.* **27**, 4778 (1991).
3. Nai-Heng Chang, Jalal Shatah, and Karen Uhlenbeck, Schrödinger maps. *Comm. Pure Appl. Math.* **53**, 590 (2000).
4. J. Daughton, Magnetoresistive memory technology, *Thin Solid Films* **216**, 162 (1992).
5. Weinan E and X. P. Wang, Numerical methods for the Landau–Lifshitz equation, *SIAM J. Numer. Anal.* **38**, 1647 (2001).
6. J. Fidler and T. Schrefl, Micromagnetic modelling—The current state of the art, *J. Phys. D: Appl. Phys.* **33**, R135 (2000).
7. B. Heinrich and J. A. C. Bland, *Ultrathin Magnetic Structures I* (Springer-Verlag, Berlin-New York, 1994).
8. B. Heinrich and J. A. C. Bland, *Ultrathin Magnetic Structures II*, Springer-Verlag, Berlin/New York, 1994.
9. R. Hertel and H. Kronmüller, Adaptive finite element techniques in three-dimensional micromagnetics modeling, *IEEE Trans. Magn.* **34**, 3922 (1998).
10. A. Hubert and R. Schäfer, *Magnetic Domains: The Analysis of Magnetic Microstructures* (Springer-Verlag/Berlin/Heidelberg/New York, 1998).

11. M. Jones and J. J. Miles, An accurate and efficient 3D micromagnetic simulation of metal evaporated tape, *J. Magn. Magn. Mater* **171**, 190 (1997).
12. W. F. Brown Jr., *Micromagnetics*. Interscience Tracts on Physics and Astronomy (Interscience Publishers, Wiley, New York/London, 1963).
13. F. Kang, On difference schemes and symplectic geometry, in *Proceedings of the 1984 Beijing Symposium on Differential Geometry and Differential Equations*, edited by F. Yang (Science Press, Beijing, 1985), pp. 42–58.
14. L. Landau and E. Lifshitz, On the theory of the dispersion of magnetic permeability in ferromagnetic bodies, *Physikalische Zeitschrift der Sowjetunion* **8**, 153 (1935).
15. Y. Nakatani, Y. Uesake, and N. Hayashi, Direct solution of the Landau–Lifshitz–Gilbert equation for micromagnetics. *Japan. J. Appl. Phys.* **28**(12), 2485 (1989).
16. Y. Nakatani, Y. Uesake, N. Hayashi, and H. Fukushima, Computer simulation of thermal fluctuation of fine particle magnetization based on Langevin equation, *J. Magn. Magn. Mater.* **168**, 347 (1997).
17. A. F. Popkov, L. L. Savchenko, N. V. Vorotnikova, S. Tehrani, and J. Shi, Edge pinning effect in single- and three-layer patterns, *Appl. Phys. Lett.* **77**(2), 277 (2000).
18. G. Prinz, Magneto-electronics, *Science* **282**, 1660 (1998).
19. W. Rave, S. Zielke, and A. Hubert, The magnetic ground state of a thin-film element, submitted for publication. *Preprint 61/1999 of MPI-MIS Leipzig*, available at <http://www.mis.mpg.de>.
20. J. J. Sanz-Serna, Symplectic integrators for Hamiltonian problems: an overview, *Acta Numerica* **1**, 243 (1991).
21. J. Shi and S. Tehrani, Edge pinned states in patterned submicron NiFeCo structures, *Appl. Phys. Lett.* **77**(11), 1692 (2000).
22. J. Shi, S. Tehrani, and M. R. Scheinfein, Geometry dependence of magnetization vortices in patterned submicron NiFe elements, *Appl. Phys. Lett.* **76**, 2588 (2000).
23. J. Shi, T. Zhu, M. Durlam, E. Chen, S. Tehrani, Y. F. Zheng, and J.-G. Zhu. End domain states and magnetization reversal in submicron magnetic structures, *IEEE Trans. Magn.* **34**, 997 (1998).
24. J. Shi, T. Zhu, S. Tehrani, Y. F. Zheng, and J.-G. Zhu, Magnetization vortices and anomalous switching in patterned NiFeCo submicron arrays, *Appl. Phys. Lett.* **74**, 2525 (1999).
25. P. Sulem, C. Sulem, and C. Bardos, On the continuous limit for a system of classical spins, *Comm. Math. Phys.* **107**(3), 431 (1986).
26. Samuel W. Yuan and Neal Bertram, Fast adaptive algorithms for micromagnetics, *IEEE Trans. Magn.* **28**(5), 2031 (1992).